Original Article

Preoperative magnetic resonance imaging identify feasibility of breast-conserving surgery for breast cancer patients

Liangsheng Liu[1#], Shanshan He[2#], Zhenhua Niu[3], Rui Yin[3], Yijun Guo[1], Zhaoxiang Dou[1], Wenjuan Ma[1], Zhaoxiang Ye[4], Hong Lu[1]

[1]Department of Breast Imaging, Tianjin Medical University Cancer Institute and Hospital, National Clinical Research Center for Cancer, Key Laboratory of Breast Cancer Prevention and Therapy, Tianjin Medical University, Ministry of Education, Key Laboratory of Cancer Prevention and Therapy, Tianjin's Clinical Research Center for Cancer, Tianjin, China; [2]Department of Breast Reconstruction, Tianjin Medical University Cancer Institute and Hospital, National Clinical Research Center for Cancer, Key Laboratory of Breast Cancer Prevention and Therapy, Tianjin Medical University, Ministry of Education, Key Laboratory of Cancer Prevention and Therapy, Tianjin's Clinical Research Center for Cancer, Tianjin, China; [3]School of Biomedical Engineering & Technology, Tianjin Medical University, Tianjin, China; [4]Department of Radiology, Tianjin Medical University Cancer Institute and Hospital, National Clinical Research Center for Cancer, Key Laboratory of Breast Cancer Prevention and Therapy, Tianjin Medical University, Ministry of Education, Key Laboratory of Cancer Prevention and Therapy, Tianjin's Clinical Research Center for Cancer, Tianjin, China

Contributions: (I) Conception and design: H Lu, Z Ye; (II) Administrative support: H Lu, Z Ye; (III) Provision of study materials or patients: L Liu, S He; (IV) Collection and assembly of data: All authors; (V) Data analysis and interpretation: L Liu, S He; (VI) Manuscript writing: All authors; (VII) Final approval of manuscript: All authors.

[#]These authors contributed equally to this work.

Correspondence to: Hong Lu, PhD. Department of Breast Imaging, Tianjin Medical University Cancer Institute and Hospital, National Clinical Research Center for Cancer, Key Laboratory of Breast Cancer Prevention and Therapy, Tianjin Medical University, Ministry of Education, Key Laboratory of Cancer Prevention and Therapy, Tianjin's Clinical Research Center for Cancer, 1 Huan-Hu West Rd., Tianjin 300181, China. Email: luhong_tianjin@163.com; Zhaoxiang Ye, PhD. Department of Radiology, Tianjin Medical University Cancer Institute and Hospital, National Clinical Research Center for Cancer, Key Laboratory of Breast Cancer Prevention and Therapy, Tianjin Medical University, Ministry of Education, Key Laboratory of Cancer Prevention and Therapy, Tianjin's Clinical Research Center for Cancer, 1 Huan-Hu West Rd., Tianjin 300181, China. Email: zye@tmu.edu.cn.

Background: Breast-conserving surgery (BCS) stands as the favored modality for treating early-stage breast cancer. Accurately forecasting the feasibility of BCS preoperatively can aid in surgical planning and reduce the rate of switching of surgical methods and reoperation. The objective of this study is to identify the radiomics features and preoperative breast magnetic resonance imaging (MRI) characteristics that are linked with positive margins following BCS in patients with breast cancer, with the ultimate aim of creating a predictive model for the feasibility of BCS.

Methods: This study included a cohort of 221 pretreatment MRI images obtained from patients with breast cancer. A total of seven MRI semantic features and 1,561 radiomics features of lesions were extracted. The feature subset was determined by eliminating redundancy and correlation based on the features of the training set. The least absolute shrinkage and selection operator (LASSO) logistic regression was then trained with this subset to classify the final BCS positive and negative margins and subsequently validated using the test set.

Results: Seven features were significant in the discrimination of cases achieving positive and negative margins. The radiomics signature achieved area under the curve (AUC), accuracy, sensitivity, and specificity of 0.760 [95% confidence interval (CI): 0.630, 0.891], 0.712 (95% CI: 0.569, 0.829), 0.882 (95% CI: 0.623, 0.979) and 0.629 (95% CI: 0.449, 0.780) in the test set, respectively. The combined model of radiomics signature and background parenchymal enhancement (BPE) demonstrated an AUC, accuracy, sensitivity, and specificity of 0.759 (95% CI: 0.628, 0.890), 0.654 (95% CI: 0.509, 0.780), 0.679 (95% CI: 0.476, 0.834) and 0.625 (95% CI: 0.408, 0.804).

Conclusions: The combination of preoperative MRI radiomics features can well predict the success of breast conserving surgery.

Keywords: Breast cancer; breast-conserving surgery (BCS); margin; magnetic resonance imaging (MRI); radiomics

Submitted Dec 13, 2023. Accepted for publication Mar 28, 2024. Published online May 27, 2024.
doi: 10.21037/gs-23-509
View this article at: https://dx.doi.org/10.21037/gs-23-509

Introduction

In cases of early-stage breast cancer, the primary decision to be made by both the patient and surgeon involves choosing between breast-conserving surgery (BCS) followed by radiation therapy or a total mastectomy with the possibility of breast reconstruction. Although there was no significant difference in survival outcomes between the two treatment options, BCS is the better choice from both a physical and psychological point of view. However, in the present scenario, a subset of patients who undergo BCS are unable to preserve their breasts due to positive margins during surgery, even secondary BCS with extended resections are performed. Accurate prediction of positive margins, especially for secondary BCS with extended resections is of significant importance when considering the feasibility of BCS. In an effort to address this issue, multiple studies have been conducted to develop predictive models and identify various clinical, pathological, and imaging predictors (1-5).

Breast magnetic resonance imaging (MRI) is commonly employed for the preoperative evaluation of breast cancer patients. Dynamic contrast-enhanced (DCE) MRI is considered the standard protocol for breast MRI, as it offers greater sensitivity and specificity when compared to mammography and ultrasound for the purposes of malignancy diagnosis, staging, and grading (6). Although various studies are committed to researching predictors of positive margins with breast DCE-MRI, including tumor size, mass type, and heterogeneous enhancement, there are inconsistencies between different studies and no relevant standards have been reported (7-9). In the meantime, radiomics is an efficacious approach for extracting pertinent information from medical images and has been progressively employed for individual-level classification in medical imaging. This technique has the potential to furnish supplementary information to medical images, thereby facilitating a more comprehensive understanding of the underlying pathology (10-14).

Our study was designed to assess the clinical and imaging factors associated with positive margins and to develop and validate a model for predicting positive margins. The ultimate goal of this model is to help prevent secondary mastectomy in patients who opt for BCS. We present this article in accordance with the STARD reporting checklist (available at https://gs.amegroups.com/article/view/10.21037/gs-23-509/rc).

Highlight box

Key findings

- Radiomics features extracted from dynamic contrast-enhanced-magnetic resonance imaging (MRI) can effectively differentiate breast cancer patients who are suitable for breast-conserving surgery (BCS) from those who are not, outperforming clinical criteria alone.

What is known and what is new?

- Higher qualitative background parenchymal enhancement (BPE) was significantly associated with an increased risk of positive margins and ultimately, failure in breast conservation surgery.
- The diagnostic performance of the combination of the radiomics score and BPE protocols in the training set and test set was 0.780 [95% confidence interval (CI): 0.699, 0.861] and 0.759 (95% CI: 0.628, 0.890), respectively.

What is the implication, and what should change now?

- We investigated a preoperative MRI-based radiomics prediction model that could offer imaging surrogates for breast cancer factors relevant to BCS in a retrospective surgical sample.

Methods

Patients and datasets

The overall study design is shown in *Figure 1*. The study was conducted in accordance with the Declaration of Helsinki (as revised in 2013). With the approval of the ethics committee of the Tianjin Medical University Cancer Institute and Hospital (approval number: bc2023027), the clinical data of 221 patients with breast cancer who underwent BCS were retrospectively analyzed. The training group included 176 patients from January 1, 2017 to June 30, 2020, and the internal validation group included 45 patients from July 1, 2012 to June 30, 2017 with a ratio of 8:2. Written informed consent for this retrospective study was waived.

Inclusion criteria for the study included: (I) histologically confirmed breast cancer; (II) all patients were suitable for BCS according to the National Comprehensive Cancer

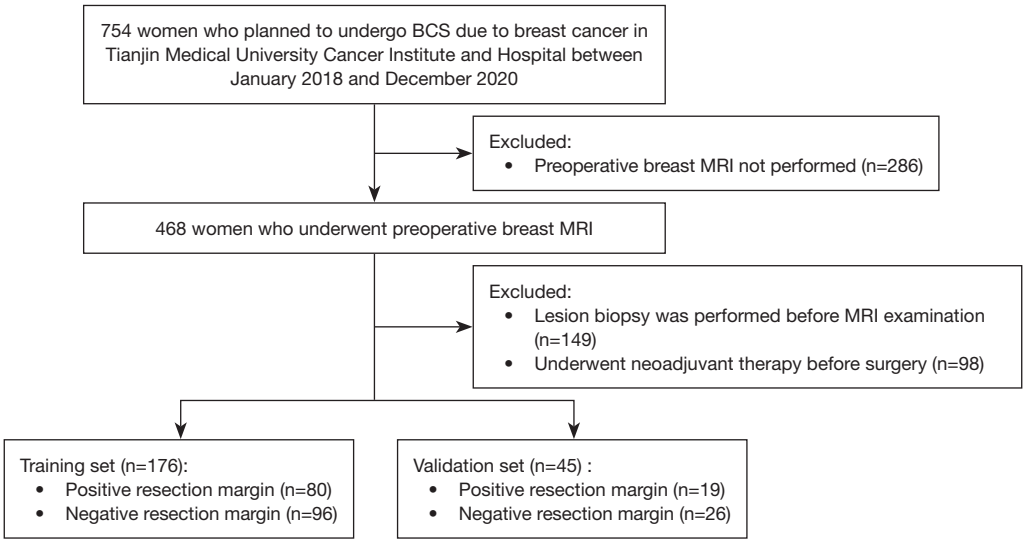

Figure 1 Study design for developing and validating a model to predict positive margins. BCS, breast-conserving surgery; MRI, magnetic resonance imaging.

Network (NCCN) guidelines (version 3.2022), and patients who underwent BCS; (III) patients with preoperative MRI examination; and (IV) access to clinical characteristics. The exclusion criteria included: (I) patients lacking complete clinical-pathologic information; (II) patients without MRI images within 1 month; (III) patients who underwent neoadjuvant therapy before surgery; (IV) patients with lesions that could not be segmented accurately; (V) patients with distant metastasis (*Figure 1*). Final BCS positive margins are defined as positive margins identified by intraoperative pathology on frozen sections of both first and secondary BCS extended resection, resulting in conversion from attempted BCS to mastectomy and failure to retain breast. Final BCS negative margins are defined as negative margins identified by intraoperative pathology on frozen sections with either first or secondary BCS extended resection, resulting in success on breast retaining.

Pathologic examination and definition of surgical margins

All patients had definite histologic results and each of the patients had been diagnosed with one of four different molecular cancer subtypes based on immune histochemical results after surgery in accordance with the 13th St. Gallen International Breast Cancer Conference [2013] Expert Panel criteria [estrogen receptor (ER)-positive or progesterone receptor (PR)-positive, human epidermal growth factor receptor 2 (HER2)-negative, and Ki67 <14% (luminal-A)]; ER-positive or PR-positive, HER2-positive or Ki67 ≥14% or PR <20% (luminal-B); ER-negative, PR-negative, and HER2-positive (HER2); ER-negative, PR-negative, and HER2-negative [triple-negative breast cancer (TNBC)]. All patients underwent intraoperative margin excision and frozen section analysis to evaluate intraoperative margins. The tumor margins were evaluated microscopically by surgical pathologists and stained prior to sectioning. Sections were sequentially sliced at 3–5 mm intervals and stained with hematoxylin and eosin. In this study, A surgical margin clearance of more than 1 mm for both invasive breast cancer and ductal carcinoma in situ (DCIS) was considered as negative margin, in accordance with the original study and NCCN clinical guidelines that defined margins <1 mm as inadequate.

MRI image acquisition and MRI semantic features

All images were obtained by a 1.5 T and 3.0 T MRI system (HDx, GE Healthcare, Tianjin, China), using an 8-channel breast dedicated coil in prone position. T1-weighted images of DCE-MRI were analyzed for this study. The extracted semantic features included MRI-reported amount of fibro glandular tissue (FGT), background parenchymal enhancement (BPE), time of intensity curve, performance in diffusion weighted imaging (DWI), skin invasion, axillary lymph node metastasis, and enhancement mode. If no descriptive information can be extracted from the diagnostic

report, one junior radiologist with 5 years of experience and an expert radiologist with 30 years of experience reviewed all images, these two radiologists were blind to pathological patterns and operation outcomes. In the case where radiologists disagreed with the features description, consensus was reached through discussion.

The region of interest (ROI) segmentation and radiomics feature extraction

Manual segmentation was performed on sagittal first phase of T1-weighted images of dynamic contrast enhanced images. The tumor lesion area was delineated on first phase image after enhancement using freely available software (ITK-SNAP; http://www.itksnap.org). The ROI of the lesion was annotated and confirmed separately by the same two radiologists mentioned above.

After tumor segmentation, a total of 1,561 radiomics features were extracted from the ROI with the open-source python package "Pyradiomics V1.3.0" (http://www.radiomics.io/pyradiomics.html), including: (I) shape-based features; (II) first-order statistics features; (III) gray level co-occurrence matrix (GLCM)-based features; (IV) gray level run-length matrix (GLRLM)-based features; (V) gray level size zone matrix (GLSZM)-based features; (VI) neighboring gray tone difference matrix (NGTDM)-based features; and (VII) gray level dependence matrix (GLDM)-based features.

Development of the radiomics signature model

We partitioned the patients into training and validation groups, with a ratio of 8:2, and employed tenfold cross-validation to assess the performance of our model in the training set. The model with the highest accuracy in the cross-validation was selected as the final model, and its predictive ability was further verified on the validation set.

Feature dimension reduction was performed to reduce the overfitting and bias of radiomics features in modeling. Firstly, Mann-Whitney *U* was used to select features that were highly correlated with the final BCS positive margins. The level of significance is 0.05 ($P<0.05$) was the threshold value. Secondly, the inter-feature coefficient (R) between all possible feature pairs was used to eliminate the high-dimensional feature redundancy. $R>0.8$ was the cutoff value for a strong correlation, excluding one of the two features with a lower P value. Then, the least absolute shrinkage and selection operator (LASSO) method was used to select the most important features with nonzero coefficients, and the radiomics score (RadScore) was calculated for each patient. Feature extraction and machine learning models were implemented in Python (3.8.13).

Evaluation of model accuracy

The relevant semantic features and RadScore were incorporated to create a radiomics nomogram model. The effectiveness of each model in the training and test sets was assessed using the area under the curve (AUC), accuracy, specificity, and sensitivity.

Statistical analysis

Continuous variables were expressed as medians and interquartile ranges depending on their distribution and were compared by using the Mann-Whitney *U* test. Categorical variables were expressed as numbers with percentages and were compared by using the χ^2 test or Fisher exact test. A univariable logistic regression analysis was performed on the training set to identify factors associated with negative margin. All statistical tests were two-sided and the level of significance was set as $\alpha = 0.05$. A multivariable logistic regression analysis was conducted by using variables selected according to their individual clinical meaning and statistical significance. The statistical analysis processes were performed in R software (version 6.1, R Foundation for Statistical Computing, Vienna, Austria). The packages used in the current study included "glmnet", "caret", "pROC", "rms" and "ggpubr".

Results

Figure 1 illustrates the flowchart of patient selection. The baseline patient characteristics are detailed in *Table 1*. A total of 221 patients met the inclusion criteria and were included in our analysis. The sample sizes of the final BCS positive resection margin and negative resection margin sets were 99 (mean age, 47 years; range, 27–69 years) and 122 (mean age, 47 years; range, 27–65 years), respectively. The final histopathological results of the surgical specimens revealed invasive ductal carcinoma (IDC) in 193 cases, DCIS in 8 cases, micropapillary carcinoma in 7 cases, mucinous carcinoma in 5 cases, invasive lobular carcinoma in 5 cases, invasive lobular carcinoma in 1 case, invasive solid papillary carcinoma in 1 case, and squamous-cell carcinoma in 1 case. The distribution of clinicopathological features did not differ between positive and negative tumor margins (*Table 1*).

Table 2 shows clinical and imaging features associated

Table 1 Difference in the clinicopathologic between breast-retaining

Characteristics	Breast-retaining		P value
	Yes	No	
Lesion size at imaging (cm), mean (SD)	2.37 (0.91)	2.60 (1.07)	0.09
Age (years), mean (SD)	47.55 (9.87)	47.61 (8.33)	0.96
Mass or NME, n (%)			0.90
Mass	92 (75.4)	73 (73.7)	
NME	30 (24.6)	26 (26.3)	
Shape, n (%)			0.15
Oval	14 (15.2)	9 (12.3)	
Round	18 (19.6)	7 (9.6)	
Irregular	60 (65.2)	57 (78.1)	
Margin, n (%)			0.36
Circumscribed	2 (2.2)	0 (0.0)	
Irregular	38 (41.3)	27 (37.0)	
Spiculated	52 (56.5)	46 (63.0)	
Internal enhancement characteristic, n (%)			0.69
Homogeneous	0 (0.0)	0 (0.0)	
Heterogeneous	24 (26.1)	22 (30.1)	
Rim enhancement	68 (73.9)	51 (69.9)	
Dark internal septations	0 (0.0)	0 (0.0)	
Distribution, n (%)			0.14
Focal	20 (66.7)	17 (65.4)	
Linear	2 (6.7)	0 (0.0)	
Segmental	7 (23.3)	4 (15.4)	
Regional	1 (3.3)	5 (19.2)	
Multiple regions	0 (0.0)	0 (0.0)	
Diffuse	0 (0.0)	0 (0.0)	
Internal enhancement patterns, n (%)			0.33
Homogeneous	1 (3.3)	0 (0.00)	
Heterogeneous	4 (13.3)	7 (28.0)	
Clumped	24 (80.0)	17 (68.0)	
Clustered ring	1 (3.3)	1 (4.0)	
Associated features, n (%)			0.81
Without	106 (86.9)	88 (88.9)	
With	16 (13.1)	11 (11.1)	
BPE symmetric or asymmetric, n (%)			0.50
Symmetric	120 (98.4)	95 (96.0)	
Asymmetric	2 (1.6)	4 (4.0)	
BPE level, n (%)			<0.001
Minimal	15 (12.3)	4 (4.0)	
Mind	74 (60.7)	34 (34.3)	
Moderate	21 (17.2)	40 (40.4)	
Marked	12 (9.8)	21 (21.2)	
Side, n (%)			0.66
Left	61 (50.4)	50 (50.5)	
Right	59 (48.8)	49 (49.5)	
Bilateral	1 (0.8)	0 (0.0)	
Quadrant, n (%)			0.28
Upper inner	57 (46.7)	36 (36.4)	
Upper outer	18 (14.8)	23 (23.2)	
Lower inner	13 (10.7)	13 (13.1)	
Lower outer	34 (27.9)	27 (27.3)	
Depth, n (%)			
Anterior	7 (5.7)	3 (3.0)	
Middle	44 (36.1)	44 (44.4)	
Posterior	71 (58.2)	52 (52.5)	
T1WI signal, n (%)			0.51
High	105 (86.1)	89 (89.9)	
Isointensity	17 (13.9)	10 (10.1)	
Low	0 (0.0)	0 (0.0)	
Fat-saturated T2WI signal, n (%)			0.54
High	7 (5.7)	4 (4.0)	
Isointensity	28 (23.0)	18 (18.2)	
Low	87 (71.3)	77 (77.8)	
TIC patterns, n (%)			0.53
Type I	11 (9.0)	5 (5.1)	
Type II	21 (17.2)	18 (18.2)	
Type III	90 (73.8)	76 (76.8)	

Table 1 *(continued)*

Characteristics	Breast-retaining		P value
	Yes	No	
FGT, n (%)			0.88
Almost entirely fat	1 (0.8)	0 (0.0)	
Scattered fibro glandular tissue	12 (9.8)	11 (11.1)	
Heterogeneous fibro glandular tissue	85 (69.7)	68 (68.7)	
Extreme fibro glandular tissue	24 (19.7)	20 (20.2)	
ER, n (%)			0.99
–	16 (13.1)	12 (12.1)	
+	106 (86.9)	87 (87.9)	
PR, n (%)			0.30
–	29 (23.8)	17 (17.2)	
+	93 (76.2)	82 (82.8)	
Ki67, n (%)			>0.99
<15%	23 (18.9)	19 (19.2)	
≥15%	99 (81.1)	80 (80.8)	
HER2, n (%)			0.10
–	55 (45.1)	33 (33.3)	
+	67 (54.9)	66 (66.7)	
Subtype, n (%)			0.78
Luminal A	13 (10.7)	8 (8.1)	
Luminal B	93 (76.2)	80 (80.8)	
HER2	12 (9.8)	7 (7.1)	
TNBC	4 (3.3)	4 (4.0)	

+, positive; –, negative. SD, standard deviation; NME, non-mass-like enhancement; BPE, background parenchymal enhancement; T1WI, T1 weighted image; T2WI, T2 weighted image; TIC, time-intensity curve; FGT, amount of fibro glandular tissue; ER, estrogen receptor; PR, progesterone receptor; HER2, human epidermal growth factor receptor 2; TNBC, triple-negative breast cancer.

with the final negative margin. In the training set, minimal BPE was used as a reference, there was no statistical difference between positive margin and mild BPE enhancement [odds ratio (OR) =1.556; 95% confidence interval (CI): 0.425, 7.426; P=0.53]. And there was statistical difference between the final positive margin and moderate (OR =4.364; 95% CI: 1.155, 21.370; P=0.041) and severe BPE enhancement (OR =4.636; 95% CI: 1.108, 24.580; P=0.047). In the test set, the AUC, accuracy, sensitivity, and specificity of the BPE enhancement protocol in predicting the final negative resection margins were 0.628 (95% CI: 0.487, 0.769), 0.654 (95% CI: 0.509, 0.780), 0.656 (95% CI: 0.468, 0.808), and 0.650 (95% CI: 0.409, 0.836) respectively.

Figure 2 shows the radiomics feature selection using LASSO logistic regression algorithm. The penalization coefficient λ in the LASSO model was tuned by using 100 iterations of cross-validation and the binomial deviance minimization criteria, and the features were selected by 10-fold cross-validation (*Figure 2A*). For the optimal λ, seven features with nonzero coefficients were selected (*Figure 2B,2C*).

In the training set, the radiomics signature was shown to have an AUC of 0.749 (95% CI: 0.664, 0.835), The cutoff value of the Youden index was calculated as 0.419, and the accuracy, sensitivity, and specificity were 0.669 (95% CI: 0.579, 0.751), 0.865 (95% CI: 0.704, 0.949) and 0.586 (95% CI: 0.476, 0.689), respectively. Similarly, in the test set, the radiomics signature achieved a significantly higher AUC (0.760; 95% CI: 0.630, 0.891), and the signature achieved an accuracy, sensitivity and specificity of 0.712 (95% CI: 0.569, 0.829), 0.882 (95% CI: 0.623, 0.979) and 0.629 (95% CI: 0.449, 0.780), respectively (*Table 3*). The DeLong test demonstrated that there was no statistically significant difference between the AUC of the training and test sets (P=0.89).

The nomogram and diagnostic performance of the combination of the RadScore and BPE protocols are shown in *Figure 3* and *Table 3*. Taking the Youden index as the cutoff value, the AUC, accuracy, sensitivity, and specificity were 0.780 (95% CI: 0.699, 0.861), 0.734 (95% CI: 0.647, 0.809), 0.769 (95% CI: 0.645, 0.861), 0.694 (95% CI: 0.560, 0.805), respectively. In the test set, it achieved the AUC, accuracy, sensitivity and specificity of 0.759 (95% CI: 0.628, 0.890), 0.654 (95% CI: 0.509, 0.780), 0.679 (95% CI: 0.476, 0.834), 0.625 (95% CI: 0.408, 0.804), respectively (*Table 3*, *Figure 3*). The combined model showed a relatively better performance than the BPE [integrated discrimination improvement (IDI) =0.137; 95% CI: 0.075, 0.199; P<0.001]. In both training and test sets, the calibration plot revealed good predictive accuracy between the actual probability and predicted probability (*Figure 3D,3E*).

Next, we analyzed the association between seven radiomics features, including three first-order features and four texture features with Kurtosis, and the three first-order

Table 2 Clinical and imaging features associated with final negative margin

Characteristics	Training set		Validation set	
	Odds ratio (95% CI)	P value	Odds ratio (95% CI)	P value
Age	0.998 (0.966, 1.031)	0.91	1.012 (0.948, 1.081)	0.72
Lesion size	1.264 (0.965, 1.673)	0.09	1.342 (0.771, 2.446)	0.31
Mass or NME				
Mass	Reference		Reference	
NME	0.947 (0.476, 1.868)	0.88	1.938 (0.489, 8.011)	0.35
Shape				
Oval	Reference		Reference	
Round	0.673 (0.170, 2.594)	0.57	0.375 (0.013, 5.915)	0.50
Irregular	1.606 (0.581, 4.703)	0.37	1.071 (0.150, 9.295)	0.95
Margin				
Circumscribed	Reference		Reference	
Irregular	4.013 (3.123, NA)	0.99	0.703 (0.147, 3.474)	0.66
Spiculated	5.918 (4.416, NA)	0.99	NA	NA
Internal enhancement characteristic				
Homogeneous	NA	NA	NA	NA
Heterogeneous	Reference		Reference	
Rim enhancement	1.033 (0.495, 2.174)	0.93	0.167 (0.008, 1.488)	0.14
Dark internal septations	NA	NA	NA	NA
Distribution				
Focal	Reference		Reference	
Linear	2.664 (NA, 7.476)	>0.99	1.500 (0.041, 57.088)	0.81
Segmental	5.667 (1.049, 2.553)	0.47	4.500 (0.295, 137.885)	0.31
Regional	4.822 (1.693, NA)	>0.99	NA	NA
Multiple regions	NA	NA	NA	NA
Diffuse	NA	NA	NA	NA
Internal enhancement patterns				
Homogeneous	Reference		Reference	
Heterogeneous	3.130 (3.023, NA)	>0.99	NA	NA
Clumped	9.391 (4.913, NA)	>0.99	1.250 (0.040, 39.013)	0.89
Clustered ring	1.000 (2.893, 1.213)	>0.99	NA	NA
Associated features				
Without	Reference		Reference	
With	0.685 (0.273, 1.635)	0.40	2.941 (0.262, 66.291)	0.39

Table 2 *(continued)*

Table 2 *(continued)*

Characteristics	Training set		Validation set	
	Odds ratio (95% CI)	P value	Odds ratio (95% CI)	P value
BPE symmetric or asymmetric				
Symmetric	Reference		Reference	
Asymmetric	3.701 (0.464, 75.642)	0.26	1.389 (0.053, 36.705)	0.82
BPE level				
Minimal	Reference		Reference	
Mind	1.556 (0.425, 7.426)	0.53	2.571 (0.330, 54.115)	0.43
Moderate	4.364 (1.155, 21.370)	0.041	12.000 (1.398, 272.304)	0.045
Marked	4.636 (1.108, 24.580)	0.047	12.000 (1.031, 333.214)	0.07
Side				
Left	Reference		Reference	
Right	0.867 (0.476, 1.575)	0.64	1.875 (0.517, 6.396)	0.30
Bilateral	NA	NA	NA	NA
Quadrant	Reference		Reference	
Upper outer	1.787 (0.756, 4.294)	0.19	3.360 (0.737, 17.087)	0.13
Lower outer	1.774 (0.658, 4.895)	0.26	1.200 (0.135, 8.560)	0.86
Lower inner	1.101 (0.535, 2.261)	0.79	2.400 (0.477, 12.840)	0.29
Lower outer	NA	NA	NA	NA
Depth	Reference		Reference	
Anterior	5.270 (0.800, 103.522)	0.14	0.714 (0.065, 7.688)	0.77
Middle	3.704 (0.568, 72.434)	0.24	0.706 (0.076, 6.560)	0.74
T1WI signal				
High	Reference		Reference	
Isointensity	0.518 (0.174, 1.381)	0.20	1.467 (0.304, 7.110)	0.62
Low	NA	NA	NA	NA
Fat-saturated T2WI signal				
High	Reference		Reference	
Isointensity	1.364 (0.308, 7.259)	0.69	0.500 (0.016, 15.744)	0.66
Low	1.824 (0.460, 8.930)	0.41	0.789 (0.030, 21.082)	0.87
TIC patterns				
Type I	Reference		Reference	
Type II	2.647 (0.518, 19.981)	0.27	1.250 (0.151, 10.587)	0.83
Type III	2.589 (0.573, 18.101)	0.25	1.275 (0.262, 7.142)	0.77

Table 2 *(continued)*

Table 2 *(continued)*

Characteristics	Training set		Validation set	
	Odds ratio (95% CI)	P value	Odds ratio (95% CI)	P value
Age				
<30 years	Reference		Reference	
30–39 years	2.667 (0.491, 20.651)	0.28	1.216 (0.000, NA)	>0.99
40–49 years	2.035 (0.411, 14.813)	0.41	4.786 (0.000, NA)	>0.99
50–59 years	2. 386 (0.459, 17.954)	0.33	5.673 (0.000, NA)	>0.99
≥60 years	1.364 (0.214, 11.599)	0.75	1.000 (0.000, 8.200)	>0.99
FGT				
Almost entirely fat	Reference		Reference	
Scattered fibro glandular tissue	2.421 (2.135, NA)	0.99	NA	NA
Heterogeneous fibro glandular tissue	1.834 (1.373, NA)	0.99	0.926 (0.185, 5.278)	0.93
Extreme fibro glandular tissue	1.412 (1.125, NA)	0.99	3.333 (0.480, 28.145)	0.24
ER				
–	Reference		Reference	
+	0.812 (0.329, 2.005)	0.65	4.286 (0.615, 86.184)	0.20
PR				
–	Reference		Reference	
+	1.320 (0.626, 2.851)	0.47	2.370 (0.574, 12.260)	0.26
Ki67				
<15%	Reference		Reference	
≥15%	1.815 (0.977, 3.424)	0.06	1.111 (0.338, 3.680)	0.86
HER2				
–	Reference		Reference	
+	1.049 (0.461, 2.433)	0.91	0.762 (0.216, 2.702)	0.67
Subtype				
Luminal A	Reference		Reference	
Luminal B	1.539 (0.506, 5.223)	0.46	1.176 (0.224, 6.789)	0.85
HER2	1.350 (0.293, 6.425)	0.70	3.333 (0.013, 4.048)	0.42
TNBC	2.400 (0.380, 16.933)	0.36	8.519 (NA, 6.225)	>0.99

CI, confidence interval; NME, non-mass-like enhancement; NA, not available; BPE, background parenchymal enhancement; T1WI, T1 weighted image; T2WI, T2 weighted image; TIC, time-intensity curve; FGT, amount of fibro glandular tissue; ER, estrogen receptor; PR, progesterone receptor; HER2, human epidermal growth factor receptor 2; TNBC, triple-negative breast cancer.

features were related to Kurtosis (*Figure 4*). It showed that the Kurtosis value of breast cancer patients with negative margins was lower than that of patients with positive margins (all P<0.05). To better understand the decisions made by the model, we selected two examples of patients with different outcomes (*Figure 5*).

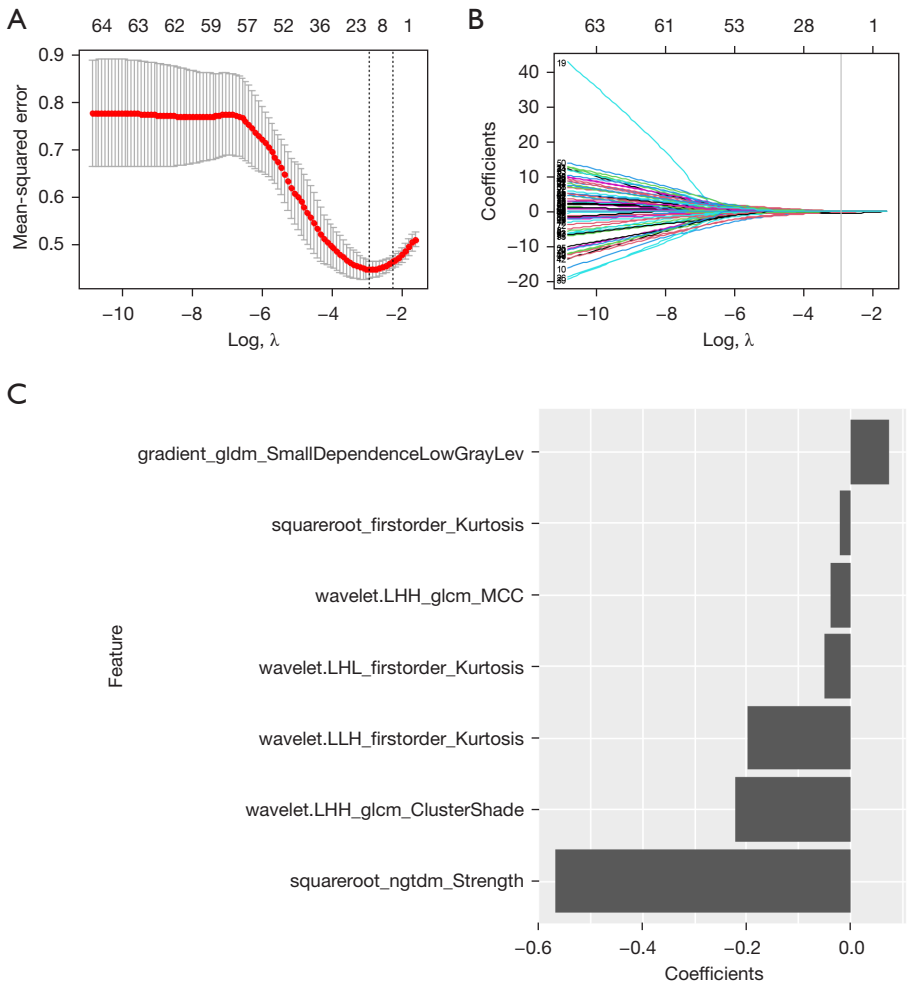

Figure 2 Flowchart demonstrating the feature selection process using the LASSO logistic regression algorithm. (A) Radiomics feature selection using LASSO logistic regression. (B) Using λ value of the minimum average binomial deviation to select features. (C) Characterization of non-zero coefficients. LHH, LHL, LLH: wavelet filters the decomposition produced at each stage, applying a combination of high-pass (H) or low-pass (L) filters. MCC, Matthews correlation coefficient; LASSO, least absolute shrinkage and selection operator.

Table 3 Performance comparison among radiomics model in the training and validation set of different image types

Cohort	AUC (95% CI)	Accuracy (95% CI)	Sensitivity (95% CI)	Specificity (95% CI)
Training set				
BPE level	0.681 (0.593, 0.770)	0.538 (0.395, 0.678)	0.701 (0.576, 0.804)	0.632 (0.493, 0.752)
RadScore	0.749 (0.664, 0.835)	0.669 (0.579, 0.751)	0.865 (0.704, 0.949)	0.586 (0.476, 0.689)
All	0.780 (0.699, 0.861)	0.734 (0.647, 0.809)	0.769 (0.645, 0.861)	0.694 (0.560, 0.805)
Test set				
BPE level	0.628 (0.487, 0.769)	0.654 (0.509, 0.780)	0.656 (0.468, 0.808)	0.650 (0.409, 0.836)
RadScore	0.760 (0.630, 0.891)	0.712 (0.569, 0.829)	0.882 (0.623, 0.979)	0.629 (0.449, 0.780)
All	0.759 (0.628, 0.890)	0.654 (0.509, 0.780)	0.679 (0.476, 0.834)	0.625 (0.408, 0.804)

AUC, area under the curve; CI, confidence interval; BPE, background parenchymal enhancement; RadScore, radiomics score.

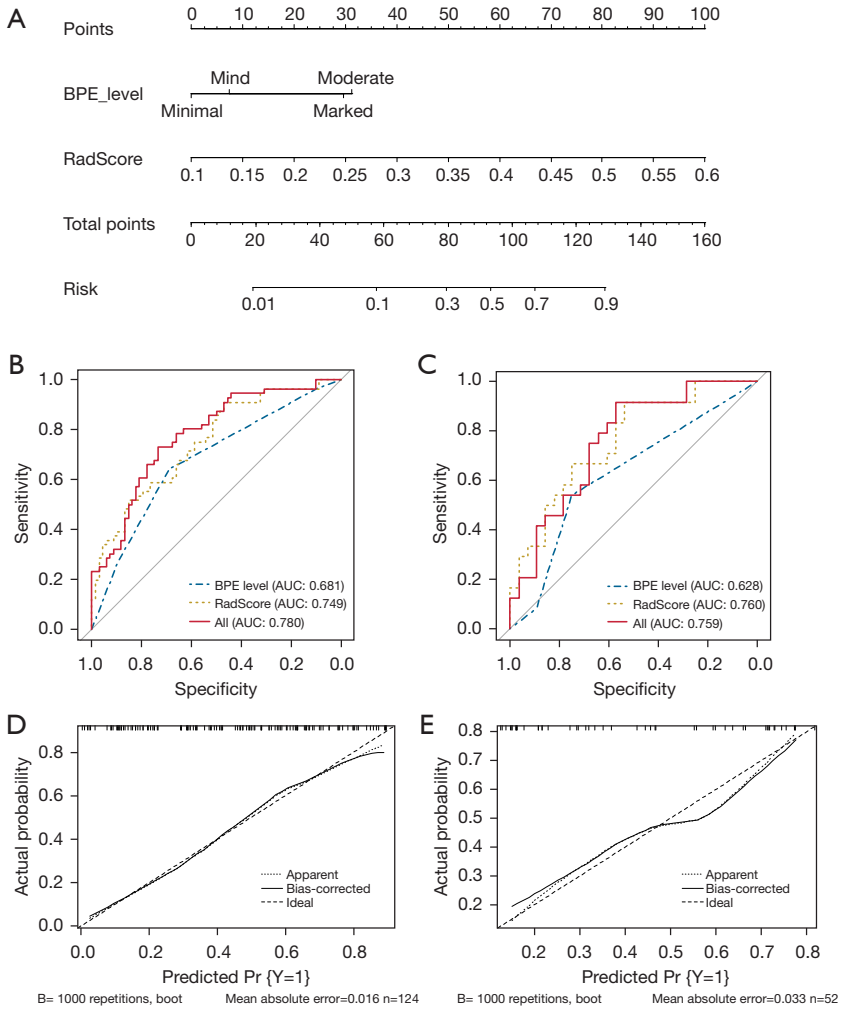

Figure 3 Integrated nomograms and diagnostic performance of the combination of the RadScore and BPE protocols. (A) A nomogram was developed in the training data set with BPE-level and RadScore. ROC and calibration curves of the nomogram for the training set (B,C) and validation set (D,E). BPE, background parenchymal enhancement; RadScore, radiomics score; AUC, area under the curve; ROC, receiver operating characteristic.

Discussion

The preoperative assessment of the feasibility of BCS by physicians directly influences the appropriateness of operative treatment for patients. For the patients without absolute contraindications, clinicians may evaluate the feasibility of BCS based on a number of factors including MRI findings and the accuracy is high currently, but a fraction of patients cannot preserve their breasts due to intraoperative positive margins found during first or secondary BCS surgery. In this study, we aimed to investigate whether a preoperative MRI-based radiomics prediction model could offer imaging surrogates for breast cancer factors relevant to BCS in a retrospective surgical sample.

The role of preoperative MRI in reducing the rate of positive resection margin in BCS patients with breast cancer remains controversial. Pleijhuis *et al.* developed a nomogram for predicting positive margins based on multicenter data and included the absence of preoperative breast MRI as one of the predictive variables (7). Kang *et al.* demonstrated a correlation between positive resection margins and tumor size on MRI, multifocality, non-mass-like enhancement (NME) with or without mass, and segmental distribution of NME (15). In a study by Bae *et al.*, preoperative breast MRI features were investigated for their association with positive or closed margins in patients with IDC. The study found that multifocal disease, non-mass enhancement

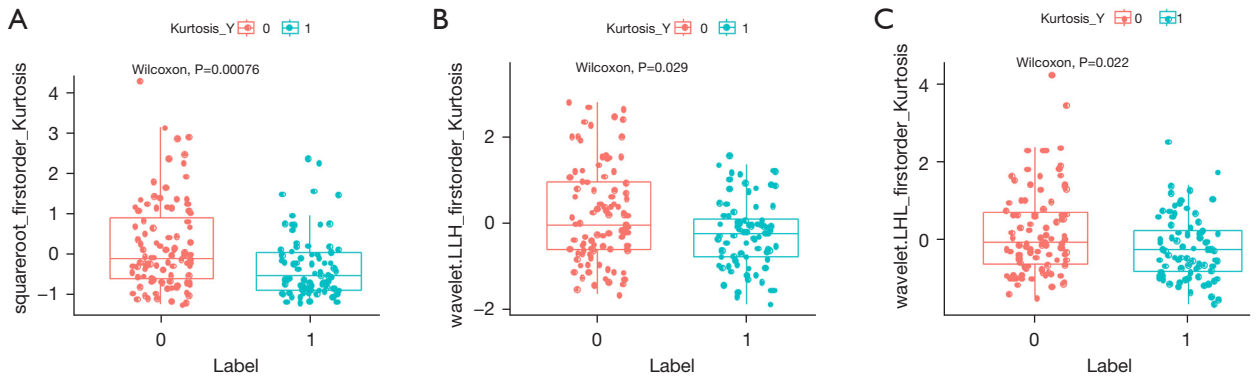

Figure 4 The correlates for radiomics features and Kurtosis. Group 0: patients with positive margins; Group 1: patients with negative margins. (A) The squareroot_firstorder_Kurtosis performed well for the differential diagnosis of positive margins from negative margins. (B) The wavelet.LLH_firstorder_Kurtosis performed well for the differential diagnosis of positive margins from negative margins. (C) The wavelet.LHL_firstorder_Kurtosis performed well for the differential diagnosis of positive margins from negative margins. LLH, LHL: wavelet filters the decomposition produced at each stage, applying a combination of high-pass (H) or low-pass (L) filters.

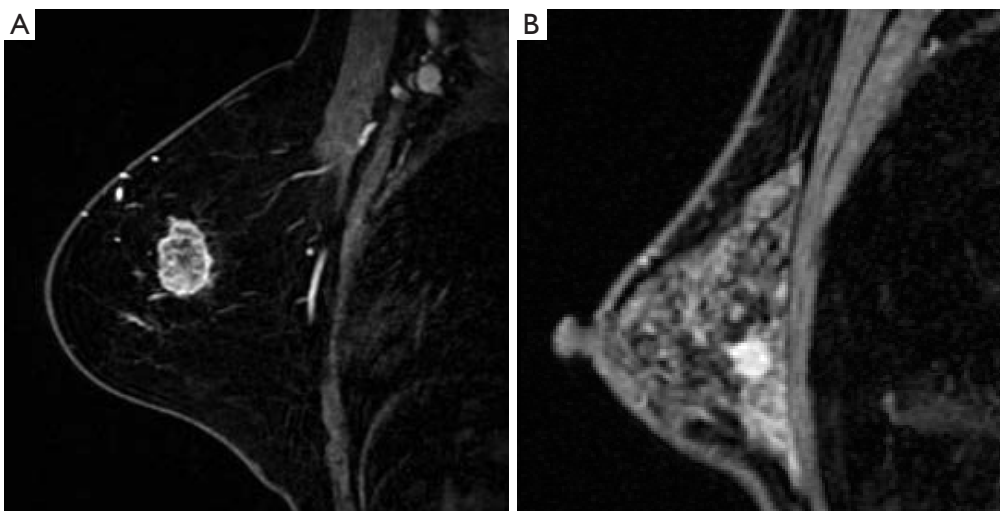

Figure 5 Examples of MRI images in two breast cancer patients. (A) View of a 60-year-old female with IDC reveal a darker glandular background on DCE-MRI, underwent breast-conserving surgery and with final negative margins. (B) View of a 41-year-old female with IDC reveal a more obvious background on DCE-MRI, underwent breast-conserving surgery but with final positive margins. MRI, magnetic resonance imaging; IDC, invasive ductal carcinoma; DCE, dynamic contrast-enhanced.

lesion, greater BPE, larger lesion size, and the presence of ductal carcinoma in situ on needle biopsy were independent predictors of positive or closed margins. Multivariate analysis revealed that NME with or without mass was an independent predictor of positive resection margins (9). However, a meta-analysis showed that preoperative breast MRI increased the overall mastectomy rate, but did not reduce the rate of lumpectomies in patients with primary breast retention (16).

Our study showed that higher qualitative BPE was significantly associated with an increased risk of positive margins and ultimately, failure in breast conservation surgery. There were also different results on the effect of BPE on the marginal state in breast preservation therapy. Specifically, one study showed that elevated BPE was an independent risk factor for a positive marginal, whereas another study suggested that elevated BPE had no impact on reoperation rates in the setting of invasive

lobular carcinoma (9,15). The disparities observed in these outcomes may be attributed to variations in the visual assessments of distinct datasets and diagnostic radiologists. Thus, it is imperative to identify an objective measure for determining whether preoperative MRI can accurately predict successful breast preservation surgery.

Radiomics is a novel approach that aims to extract high-throughput, quantitative imaging features from medical images in order to complement traditional biomarkers, thereby aiding clinical decision-making. As the use of DCE-MRI in breast cancer screening is increasing, recent studies have demonstrated a correlation between the radiological characteristics of DCE-MRI and breast cancer risk, chemotherapy effectiveness, and prognosis (17-22). In this study, the radiomics analysis finally obtained seven radiomics features, including three first-order features and four texture features, and the three first-order features related to Kurtosis. The study revealed that the Kurtosis value of breast cancer patients with negative margins was comparatively lower than those with positive margins. Kurtosis is a measure of the 'peakedness' of the distribution of values in the image ROI, and it is a measure of whether the values are heavy-tailed or light-tailed relative to a normal distribution. In the context of breast cancer imaging, high kurtosis values may indicate a higher degree of vascularity or blood supply in the tumor, which has been found to be associated with more aggressive disease characteristics.

There were some limitations to our study. Firstly, it was a single-center retrospective study conducted over a limited time period, which may have introduced selection bias between women who received preoperative MRI and those who did not undergo BCS. Secondly, our radiomics model was constructed and validated using MRI data from different field strengths (1.5 T and 3.0 T) and vendors, which may have impacted the model's performance. Thirdly, due to the lack of preoperative biopsy in some patients, pathologic results were not included in the analysis. Fourthly, our radiomics analysis was limited to the first phase of images after MRI enhancement, and including other phases of images could potentially improve the prediction accuracy in future studies.

Conclusions

In conclusion, our study revealed that radiomics features extracted from DCE-MRI can effectively differentiate breast cancer patients who are suitable for BCS from those who are not, outperforming clinical criteria alone. These findings demonstrate the potential use of imaging algorithms to enhance patient care and aid in patient selection for clinical trials. Additional ongoing efforts by our group include the acquisition of external-testing data from other centers and imaging platforms.

Acknowledgments

Funding: The present study was sponsored by the Natural Science Foundation of China (Nos. 82072004, 82172025, 81801781).

Footnote

Reporting Checklist: The authors have completed the STARD reporting checklist. Available at https://gs.amegroups.com/article/view/10.21037/gs-23-509/rc

Data Sharing Statement: Available at https://gs.amegroups.com/article/view/10.21037/gs-23-509/dss

Peer Review File: Available at https://gs.amegroups.com/article/view/10.21037/gs-23-509/prf

Conflicts of Interest: All authors have completed the ICMJE uniform disclosure form (available at https://gs.amegroups.com/article/view/10.21037/gs-23-509/coif). The authors have no conflicts of interest to declare.

Ethical Statement: The authors are accountable for all aspects of the work in ensuring that questions related to the accuracy or integrity of any part of the work are appropriately investigated and resolved. The study was conducted in accordance with the Declaration of Helsinki (as revised in 2013). This retrospective study's protocol was approved by the ethics committee of the Tianjin Medical University Cancer Institute and Hospital (approval number: bc2023027), and written informed consent for this retrospective study was waived.

References

1. Qu YH, He YJ, Li XT, et al. Preoperative MRI features predict failed breast-conserving surgery: construction of a predictive model. Transl Cancer Res 2022;11:639-48.
2. Jung JJ, Kang E, Kim EK, et al. External validation and modification of nomogram for predicting positive resection margins before breast conserving surgery. Breast Cancer Res Treat 2020;183:373-80.
3. Simpson D, Allan J, McFall B. Radiological Underestimation of Tumor Size Influences the Success Rate of Re-Excision after Breast-conserving Surgery. Eur J Breast Health 2021;17:363-70.
4. Braunstein LZ, Taghian AG, Niemierko A, et al. Breast-cancer subtype, age, and lymph node status as predictors of local recurrence following breast-conserving therapy. Breast Cancer Res Treat 2017;161:173-9.
5. van Deurzen CH. Predictors of Surgical Margin Following Breast-Conserving Surgery: A Large Population-Based Cohort Study. Ann Surg Oncol 2016;23:627-33.
6. Lehman CD. Magnetic resonance imaging in the evaluation of ductal carcinoma in situ. J Natl Cancer Inst Monogr 2010;2010:150-1.
7. Pleijhuis RG, Kwast AB, Jansen L, et al. A validated web-based nomogram for predicting positive surgical margins following breast-conserving surgery as a preoperative tool for clinical decision-making. Breast 2013;22:773-9.
8. Kurniawan ED, Wong MH, Windle I, et al. Predictors of surgical margin status in breast-conserving surgery within a breast screening program. Ann Surg Oncol 2008;15:2542-9.
9. Bae MS, Bernard-Davila B, Sung JS, et al. Preoperative breast MRI features associated with positive or close margins in breast-conserving surgery. Eur J Radiol 2019;117:171-7.
10. Shin J, Seo N, Baek SE, et al. MRI Radiomics Model Predicts Pathologic Complete Response of Rectal Cancer Following Chemoradiotherapy. Radiology 2022;303:351-8.
11. Mao N, Shi Y, Lian C, et al. Intratumoral and peritumoral radiomics for preoperative prediction of neoadjuvant chemotherapy effect in breast cancer based on contrast-enhanced spectral mammography. Eur Radiol 2022;32:3207-19.
12. Dean PB. Radiomics and Breast Cancer Management. Acad Radiol 2022;29:1783-5.
13. Daimiel Naranjo I, Gibbs P, Reiner JS, et al. Breast Lesion Classification with Multiparametric Breast MRI Using Radiomics and Machine Learning: A Comparison with Radiologists' Performance. Cancers (Basel) 2022;14:1743.
14. Peng L, Zhang X, Liu J, et al. MRI-radiomics-clinical-based nomogram for prenatal prediction of the placenta accreta spectrum disorders. Eur Radiol 2022;32:7532-43.
15. Kang JH, Youk JH, Kim JA, et al. Identification of Preoperative Magnetic Resonance Imaging Features Associated with Positive Resection Margins in Breast Cancer: A Retrospective Study. Korean J Radiol 2018;19:897-904.
16. Houssami N, Turner R, Morrow M. Preoperative magnetic resonance imaging in breast cancer: meta-analysis of surgical outcomes. Ann Surg 2013;257:249-55.
17. Bian T, Wu Z, Lin Q, et al. Evaluating Tumor-Infiltrating Lymphocytes in Breast Cancer Using Preoperative MRI-Based Radiomics. J Magn Reson Imaging 2022;55:772-84.
18. Yoshida K, Kawashima H, Kannon T, et al. Prediction of pathological complete response to neoadjuvant chemotherapy in breast cancer using radiomics of pretreatment dynamic contrast-enhanced MRI. Magn Reson Imaging 2022;92:19-25.
19. Wang S, Wei Y, Li Z, et al. Development and Validation of an MRI Radiomics-Based Signature to Predict Histological Grade in Patients with Invasive Breast Cancer. Breast Cancer (Dove Med Press) 2022;14:335-42.
20. Song D, Yang F, Zhang Y, et al. Dynamic contrast-enhanced MRI radiomics nomogram for predicting axillary lymph node metastasis in breast cancer. Cancer Imaging 2022;22:17.
21. Jiang M, Li CL, Luo XM, et al. An MRI-based Radiomics Approach to Improve Breast Cancer Histological Grading. Acad Radiol 2023;30:1794-804.
22. Li H, Whitney HM, Ji Y, et al. Impact of continuous learning on diagnostic breast MRI AI: evaluation on an independent clinical dataset. J Med Imaging (Bellingham) 2022;9:034502.

Cite this article as: Liu L, He S, Niu Z, Yin R, Guo Y, Dou Z, Ma W, Ye Z, Lu H. Preoperative magnetic resonance imaging identify feasibility of breast-conserving surgery for breast cancer patients. Gland Surg 2024;13(5):640-653. doi: 10.21037/gs-23-509